Supplementary Material

Energy-efficient electrochemical ammonia production from dilute nitrate solution

Keon-Han Kim[a] Heebin Lee,[b] Xiaopeng Huang, [a,c] Jong Hui Choi,[b] Chunping Chen,[a] Jeung Ku Kang[b] and Dermot O'Hare[a*]*

[a]Department of Chemistry
Chemical Research Laboratory, University of Oxford
OX1 3TA, United Kingdom

[b]Department of Materials Science and Engineering
Korea Advanced Institute of Science and Technology (KAIST)
34141, Republic of Korea

[c]Department of Chemistry
Faculty of Arts and Sciences, Beijing Normal University, Zhuhai
519087, China

*Corresponding authors : jeung@kaist.ac.kr, dermot.ohare@chem.ox.ac.uk

Table of Contents

I. Methods detail

I-1. Preparation

Chemicals Nickel chloride (Sigma-Aldrich, >98 %), cobalt chloride (Sigma-Aldrich, >97 %), zinc chloride (Sigma-Aldrich, >98 %), magnesium chloride (Sigma-Aldrich, >98 %), vanadium chloride (Sigma-Aldrich, >97 %), iron chloride (Sigma-Aldrich, >97 %), aluminium chloride (Sigma-Aldrich, >98 %), urea (Sigma-Aldrich, >99.5 %), sodium carbonate (Sigma-Aldrich, >99.5 %), sodium hydroxide (Sigma-Aldrich, >98 %), potassium hydroxide (Sigma-Aldrich, >85%), perfluorinated resin solution containing Nafion™ 1100W (Sigma-Aldrich), hydrochloric acid (Sigma-Aldrich, >37 %), potassium nitrate (Sigma-Aldrich, >99 %), potassium nitrite (Sigma-Aldrich, >96 %), dimethyl sulfoxide (DMSO, Sigma-Aldrich, anhydrous, >99.9%), deuterium oxide (Sigma-Aldrich, >99.9 atom % D), salicylic acid (Sigma-Aldrich, >99 %), sodium citrate monobasic (Sigma-Aldrich, >99 %), sodium hypochlorite (Sigma-Aldrich, 6-14 % active chlorine), sodium nitroferricyanide (Sigma-Aldrich, >99 %), sulfanilamide (Sigma-Aldrich, >99 %), N-(1-Naphthyl) ethylenediamine dihydrochloride (Sigma-Aldrich, >99 %), sulfamic acid (Sigma-Aldrich, >99.3 %). All reagents were used as received in air without further purification.

I-2. Structural characterizations

The powder X-ray diffraction (PXRD) spectra were gained using a Bruker D8 Discovery instrument using Cu Kα radiation (λ = 1.5406 Å) from 2θ = 3° to 70° with a 0.02° step size. Infrared spectra were collected on a Vertex 80 Spectrometer, equipped with a high performance DuraSamp1IR II diamond accessory of attenuated total reflection (ATR) mode with a range of 600 cm^{-1} ~ 4000 cm^{-1}. The *ex situ* synchrotron X-ray absorption measurements were performed at 10 C beamline of Pohang Accelerator Laboratory (PAL, Republic of Korea), and a calibration of each metal K-edge spectrum was accomplished by employing the reference spectrum from the corresponding each metal foil. The X-ray Photon Spectroscopy (XPS) results were obtained by using the K-alpha instrument (Thermo Scientific) equipped with the Al Kα micro-focused X-ray monochromator (1487 eV). Nitrogen adsorption–desorption isotherms and pore-size distribution were recorded at 77.4 K in a Micrometric Tristar surface characterization analyzer. Samples were degassed at 80 °C for 12 hours under vacuum prior to analysis. The UV-Vis spectrum was obtained using a V-570 UV-vis spectrometer (Jasco, Japan). The transmission electron microscopy (TEM) images were gained by a JEM-ARM200F model (JEOL LTD., Japan) and the Cs-

corrected scanning TEM (STEM) measurements were performed for the energy dispersive X-ray spectrometer (EDS) mapping images using a BRUKER QUANTAX EDS. The ESR data were taken by X-band (9.48 GHz) ESR spectrometer (JEOL, JES-FA200) operating at room temperature.

II. Supplementary structural characterisations

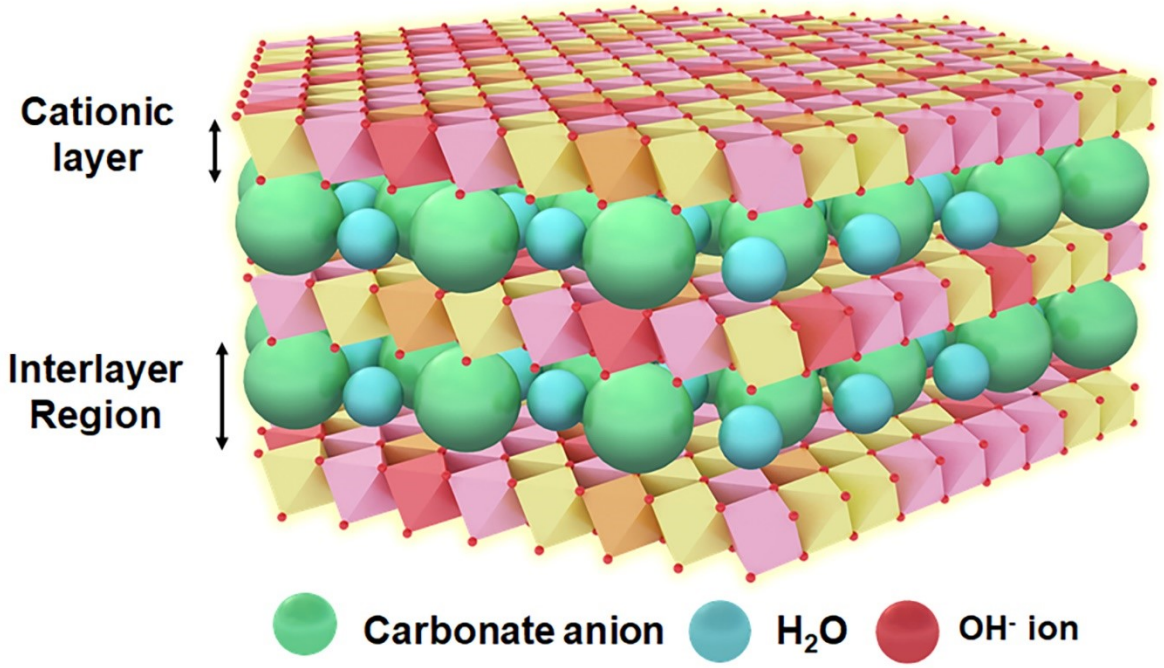

Fig. S1 | A schematic image of layered double hydroxide structure. In the cationic layers, different types of metal cations can be included in LDH structure.

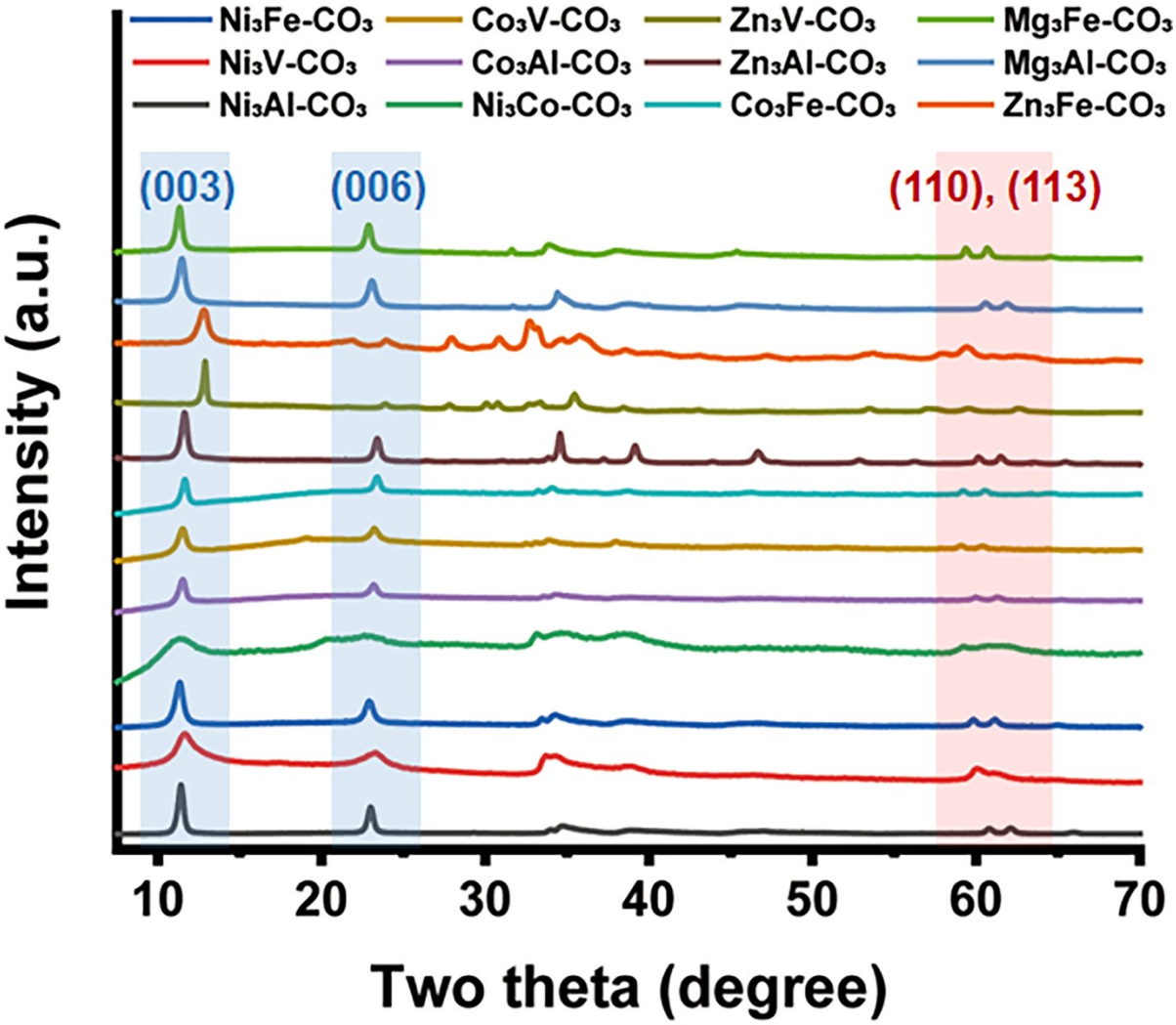

Fig. S2 | PXRD patterns for different LDHs.

A

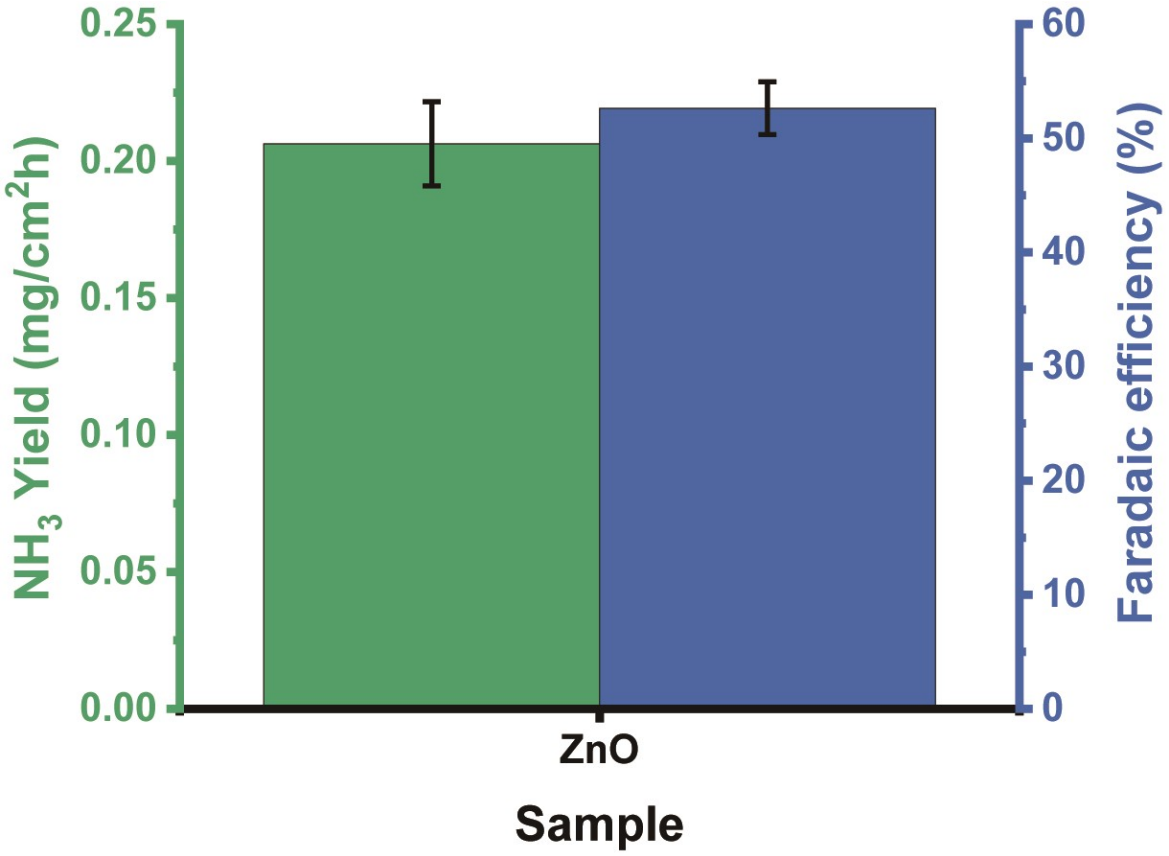

Fig. S3 | NH_3 productivity and faradaic efficiency (%) using pure ZnO/Cu foam electrode. Electrocatalysis reactions was operated at 1 M KOH electrolyte with 5 mM of KNO_3 at –0.2 V (vs RHE).

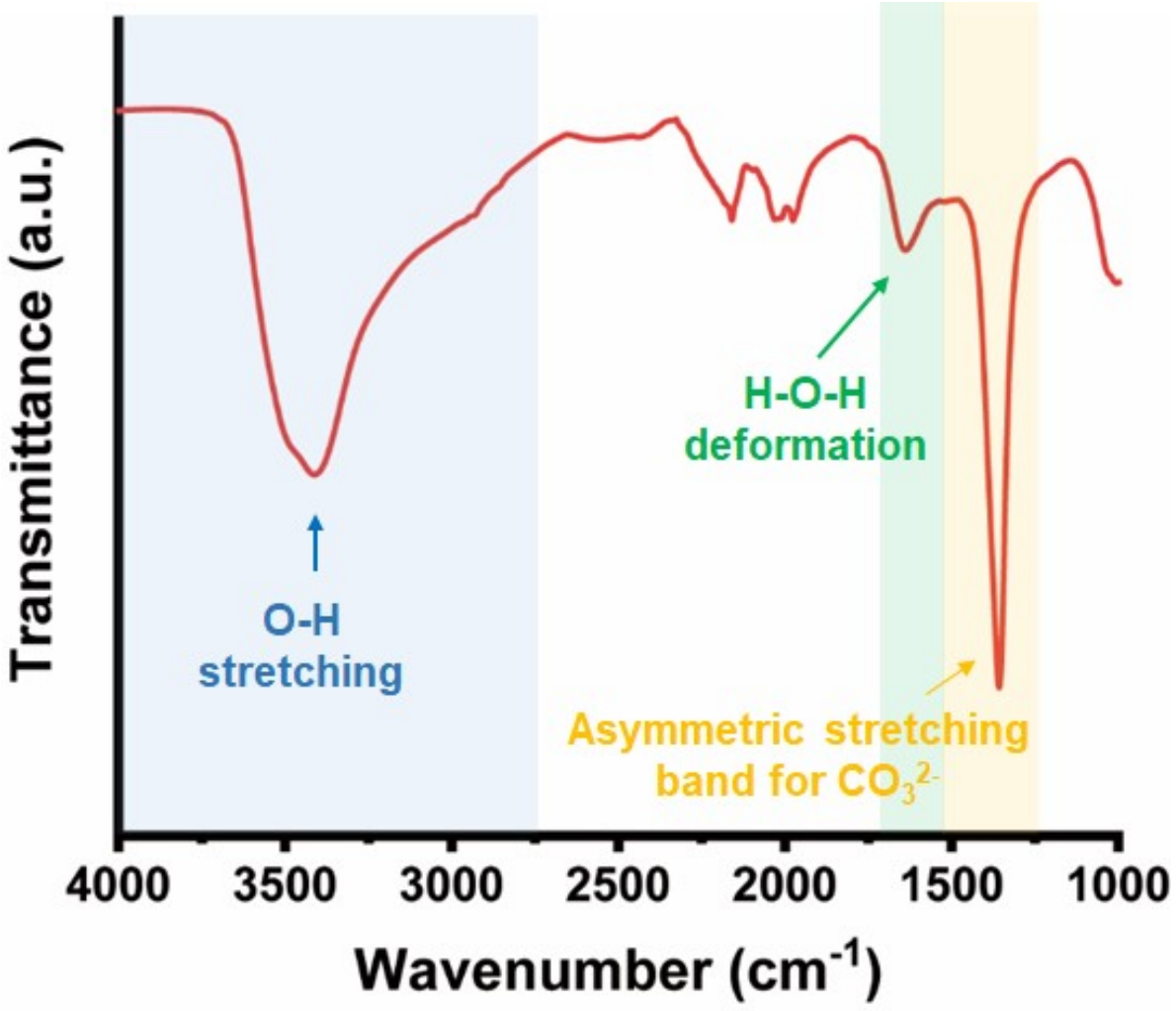

Fig. S4 | FT-IR spectrum of the Ni_3Fe-CO_3 LDH.

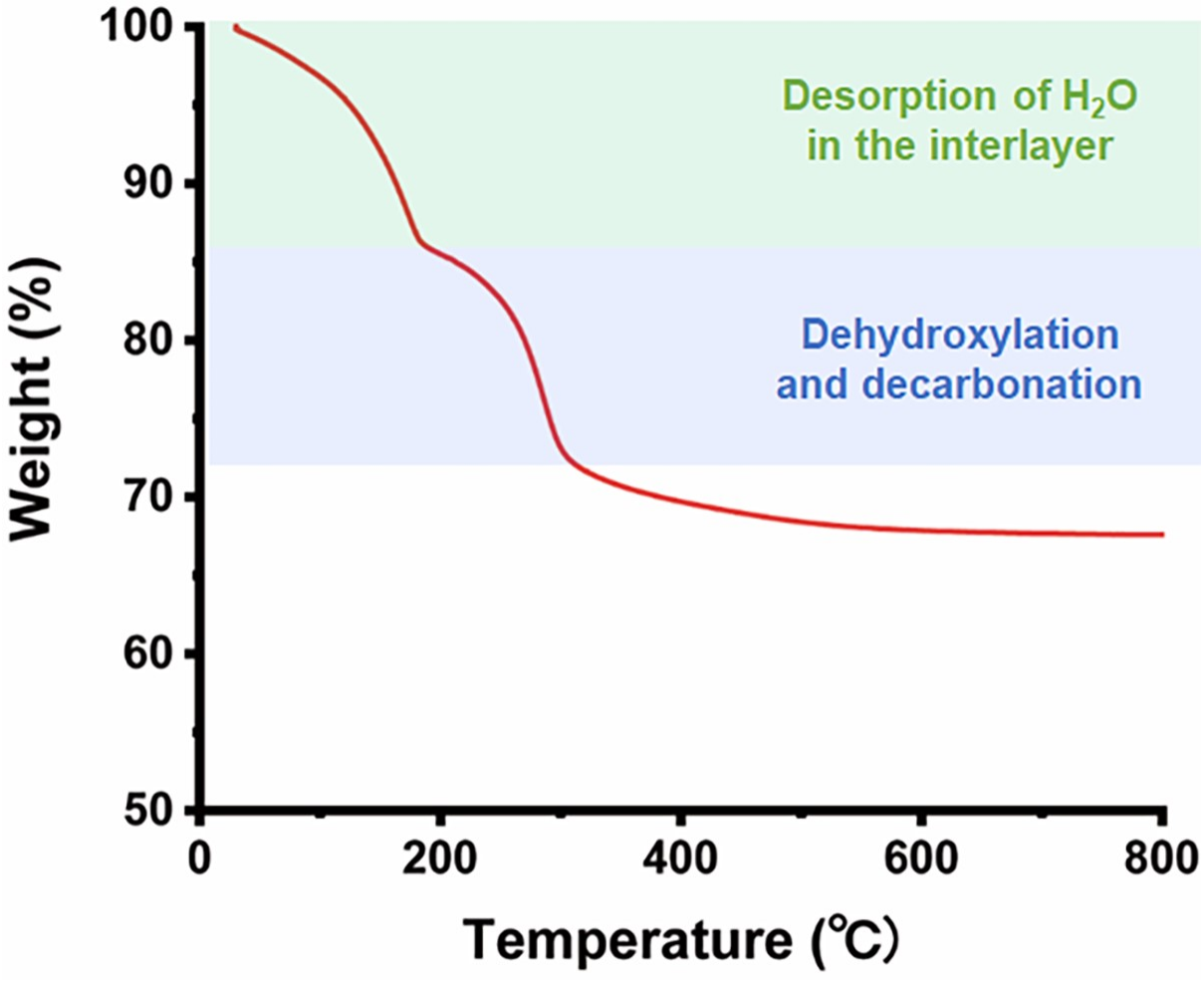

Fig. S5 | TGA curve of the Ni_3Fe-CO_3 LDH.

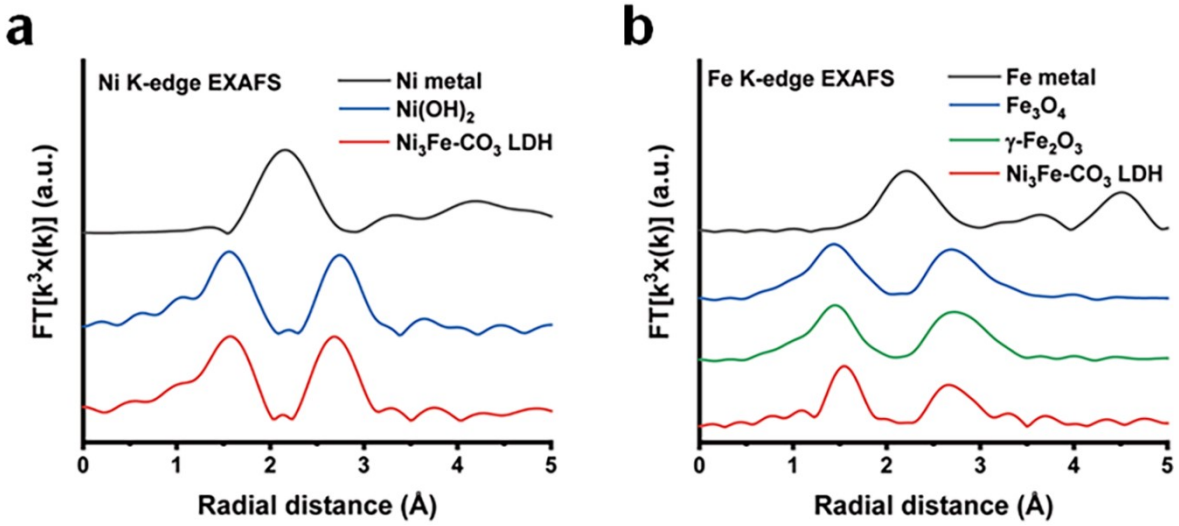

Fig. S6 | (a) Ni K-edge and (b) Fe K-edge FT-EXAFS of the Ni_3Fe-CO_3 LDH with selected reference materials.

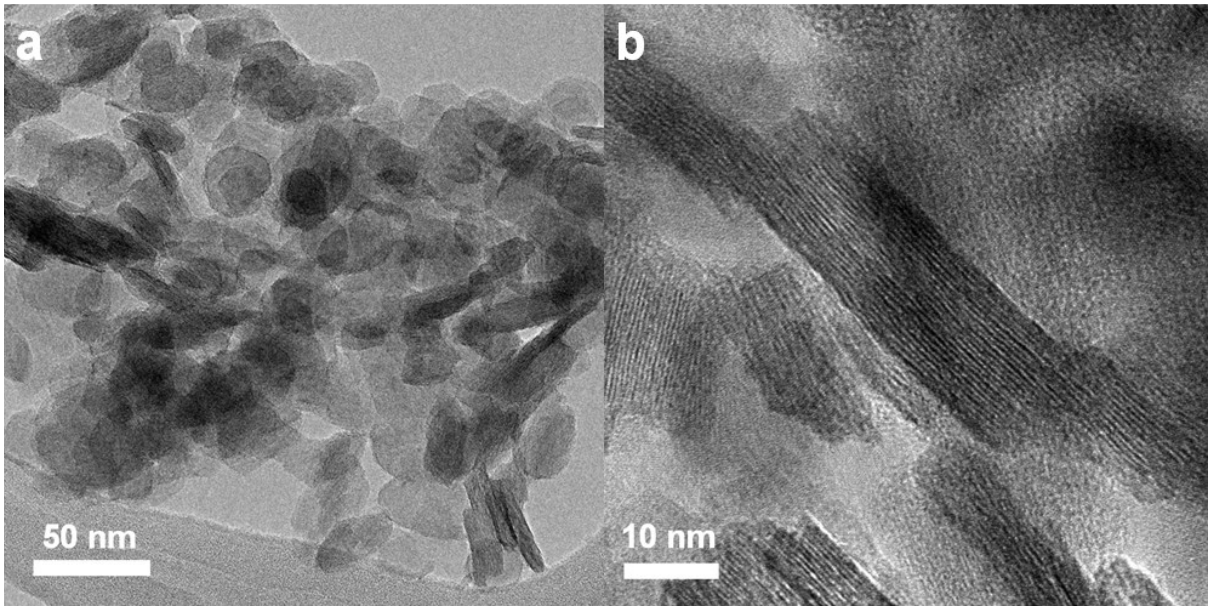

Fig. S7 | TEM and HR-TEM images of the Ni_3Fe-CO_3 LDH.

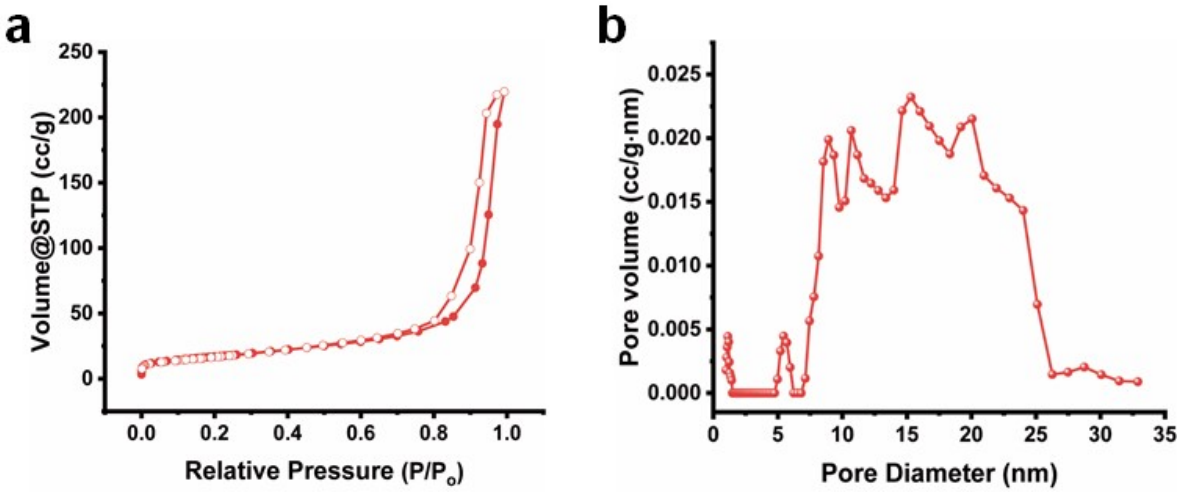

Fig. S8 | (a) N_2 adsorption-desorption isotherm and (b) pore size distribution of the Ni_3Fe-CO_3 LDH.

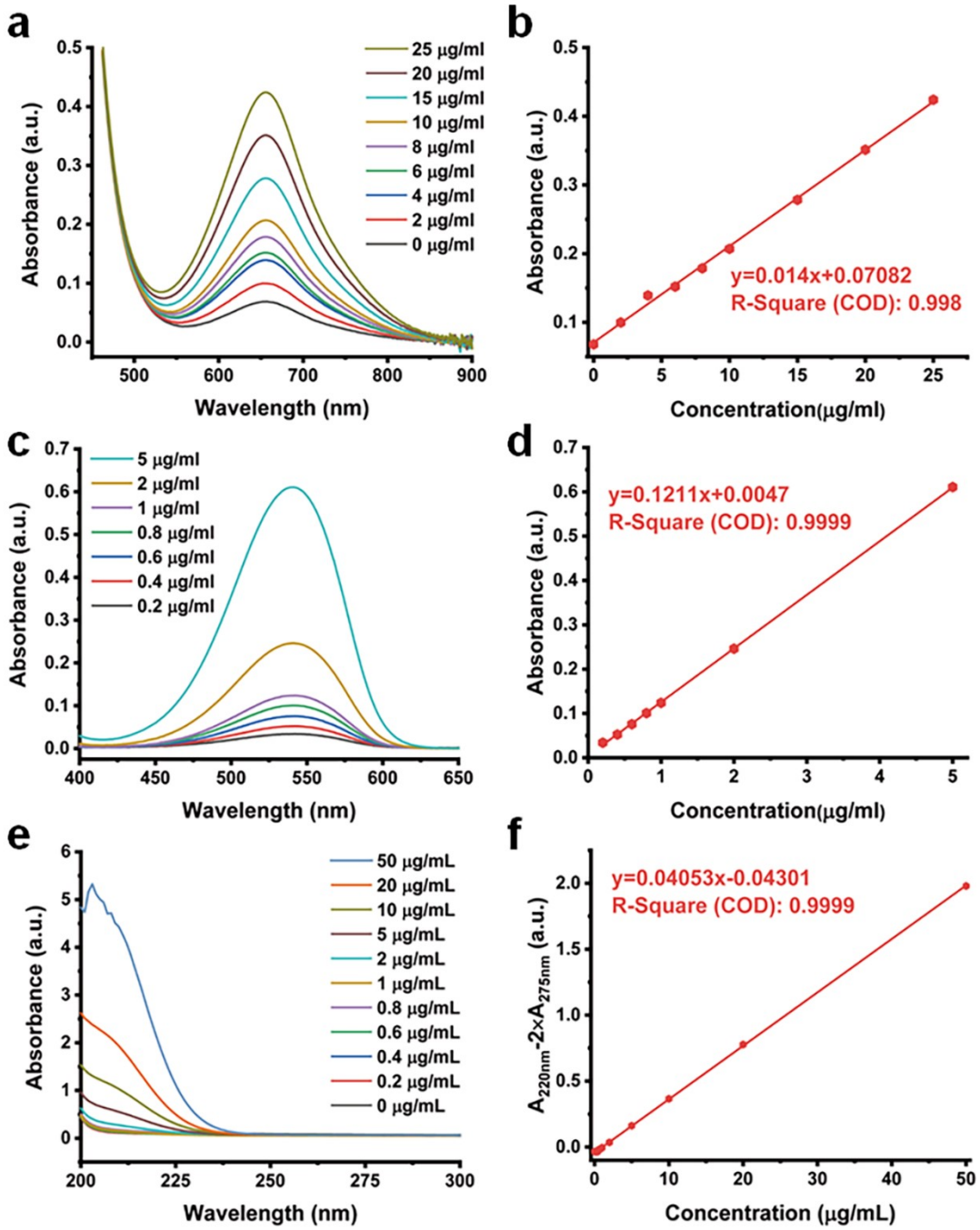

Fig. S9 | Determining the amount of NH_3 and NO_2^-. (a) UV-vis absorption spectrum changes of NH_3 amount. **(b)** Calibration curve. (y = a*x + b, a = 0.014, b = 0.07082, COD = 0.998) **(c)** UV-vis absorption spectrum changes of [NO_2^-]. **(d)** Calibration curve. (y = a*x + b, a = 0.1211, b = 0.0047, COD = 0.9999) **(e)** UV-vis absorption spectrum as function of [NO_3^-] . **(e)** Calibration curve. (y = a*x + b, a = 0.04053, b = –0.04301, COD = 0.9999)

III. Supplementary electrochemical analysis

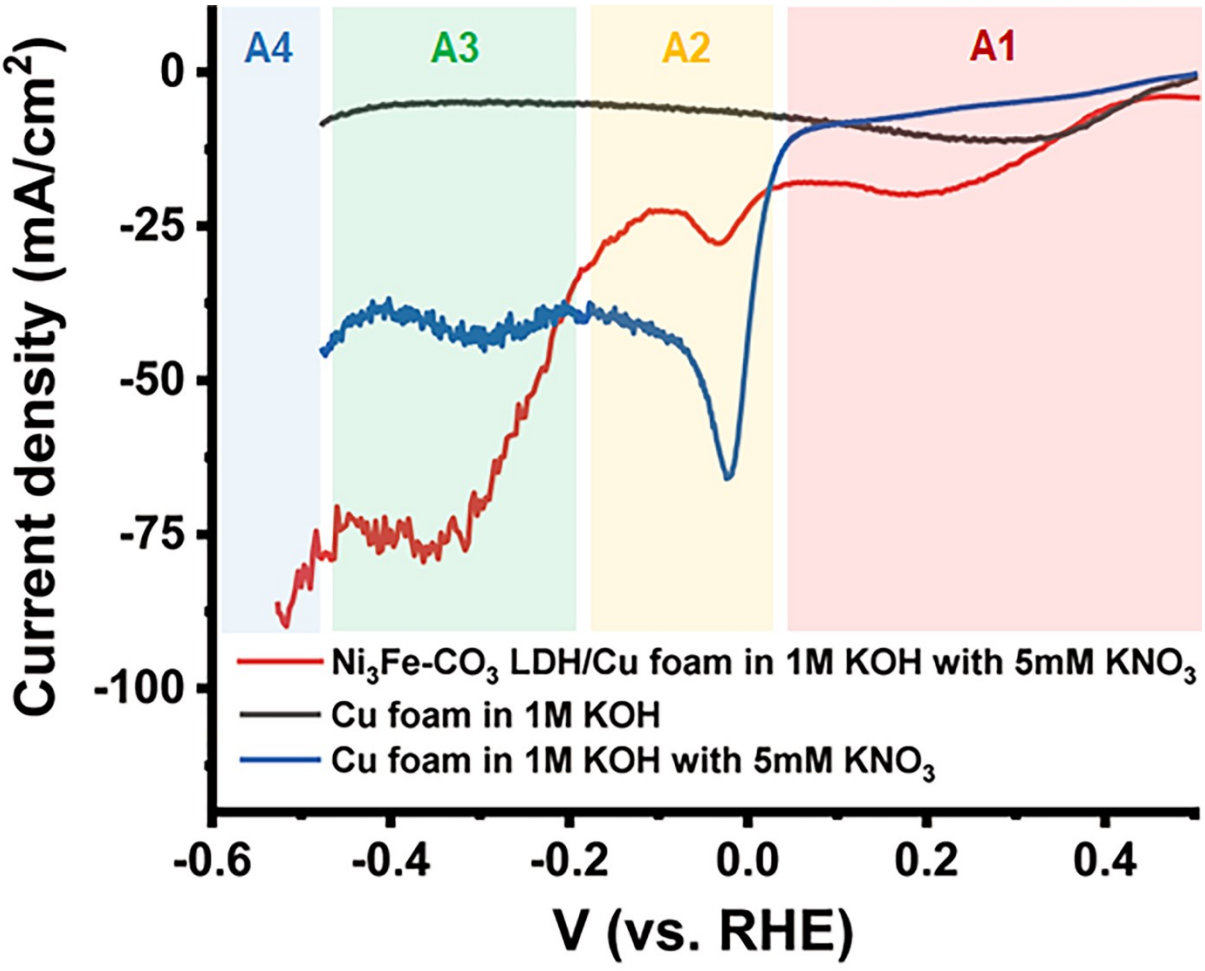

Fig. S10 | LSV curves for Ni_3Fe-CO_3 LDH/Cu foam and Cu foam with/without KNO_3

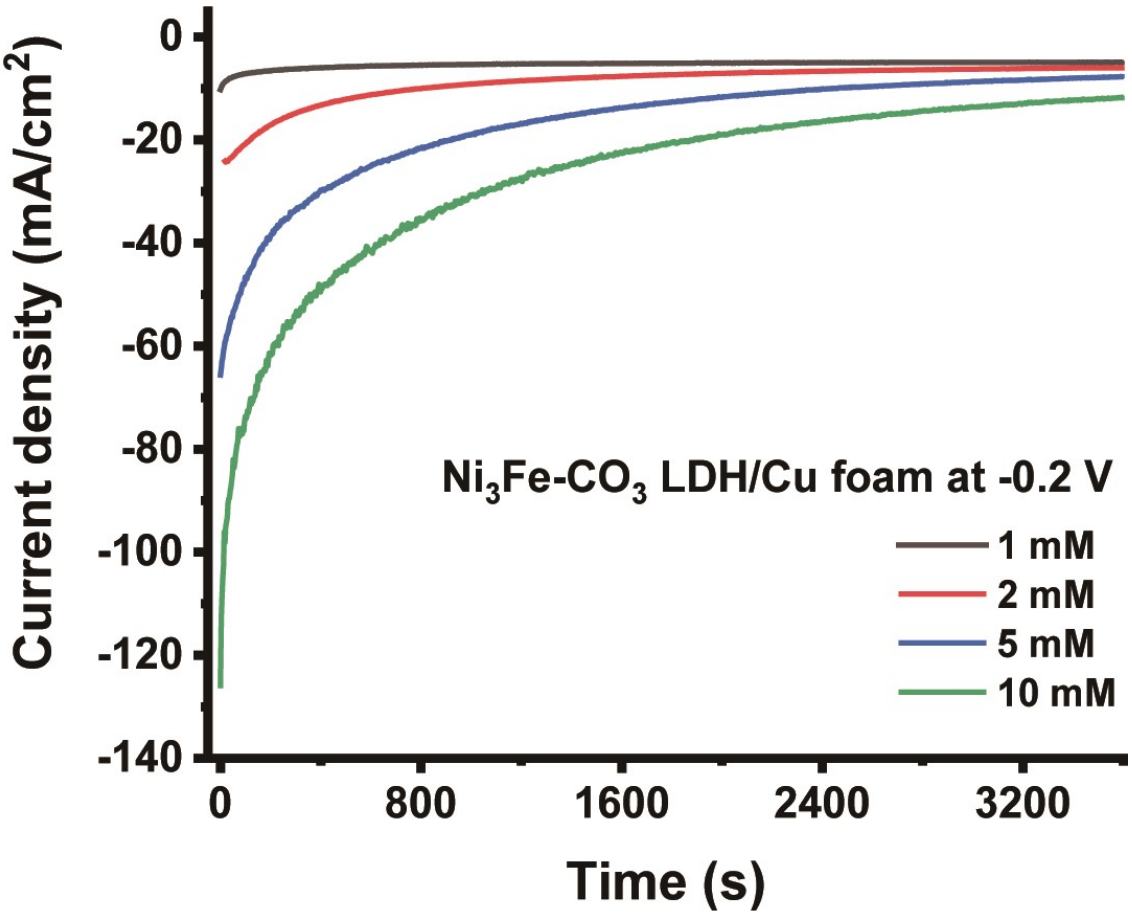

Fig. S11 | i-t curve depending on the different concentration of KNO_3.

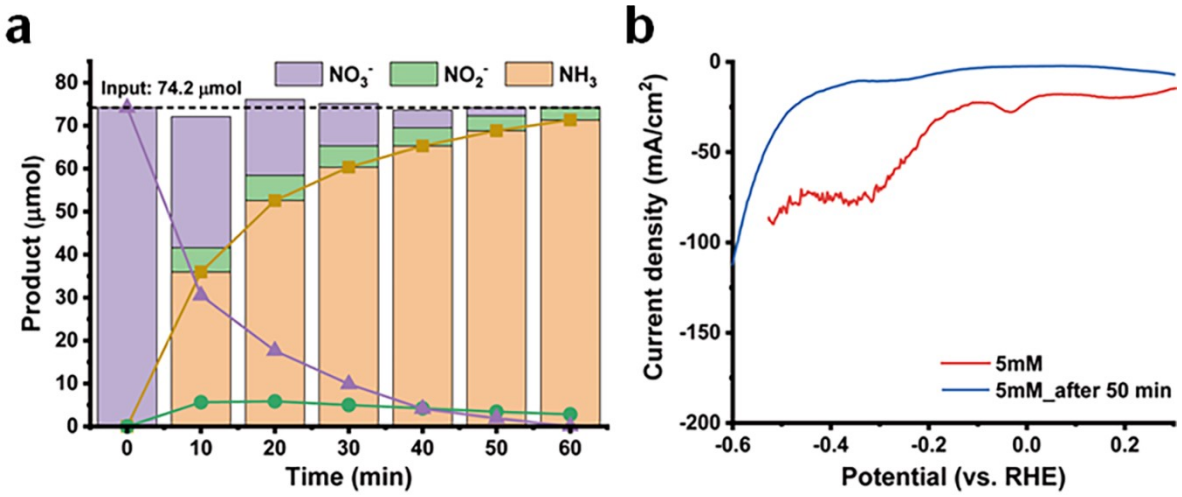

Fig. S12 | (a) Time-dependent product variation analysis and (b) LSV curves of the Ni_3Fe-CO_3 LDH/Cu foam before electrochemical NitRR and after 50 min of reaction under 1 M KOH with 5 mM KNO_3.

IV. Supplementary X-ray techniques

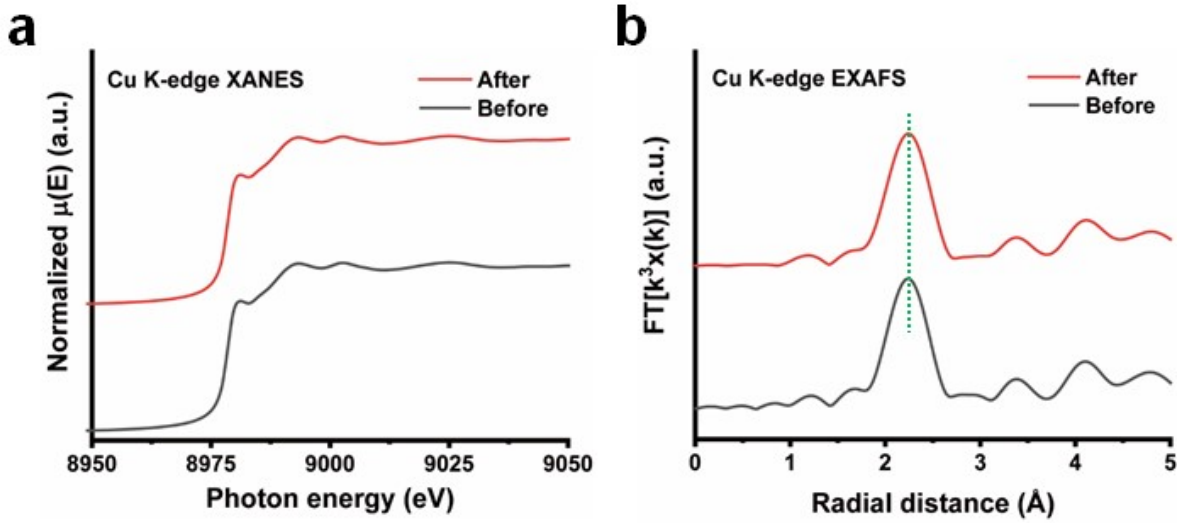

Fig. S13 | Ex-situ Cu K-edge XAS analysis. (a) Cu K-edge XANES spectra and **(b)** Cu K-edge EXAFS spectra before/after electrochemical nitrate reduction. The after-RXN sample has analysed after 1 cycle of electrochemical reaction conducted by chronoamperometric technique for an hour at –0.2 V (vs RHE) in 1 M KOH with 5 mM of KNO_3.

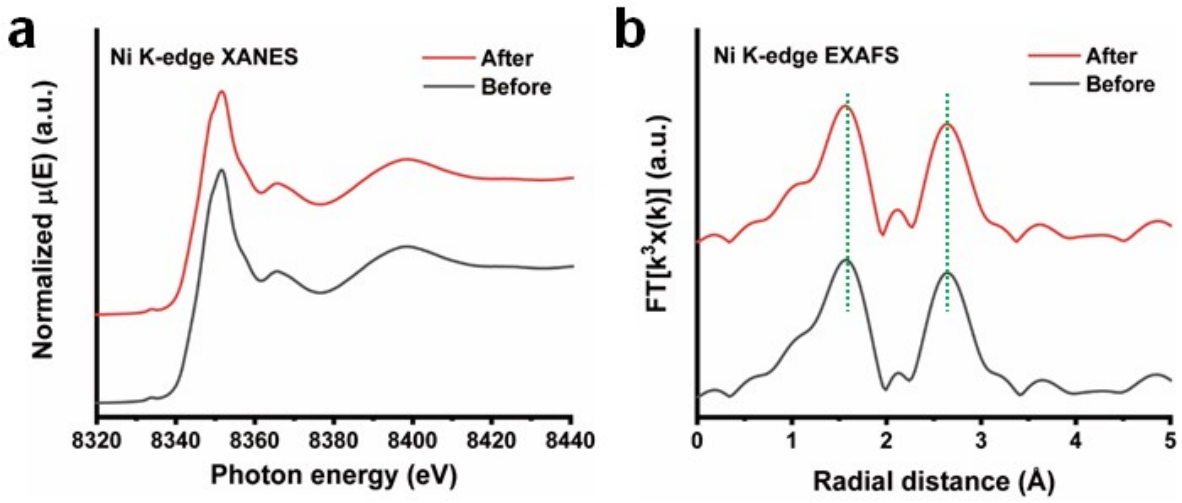

Fig. S14 | **Ex-situ Ni K-edge XAS analysis. (a)** Ni K-edge XANES spectra and **(b)** Ni K-edge EXAFS spectra before/after electrochemical nitrate reduction. The after-RXN sample has analysed after 1 cycle of the electrochemical reaction conducted by chronoamperometric technique for an hour at –0.2 V (vs RHE) in 1 M KOH with 5 mM of KNO_3.

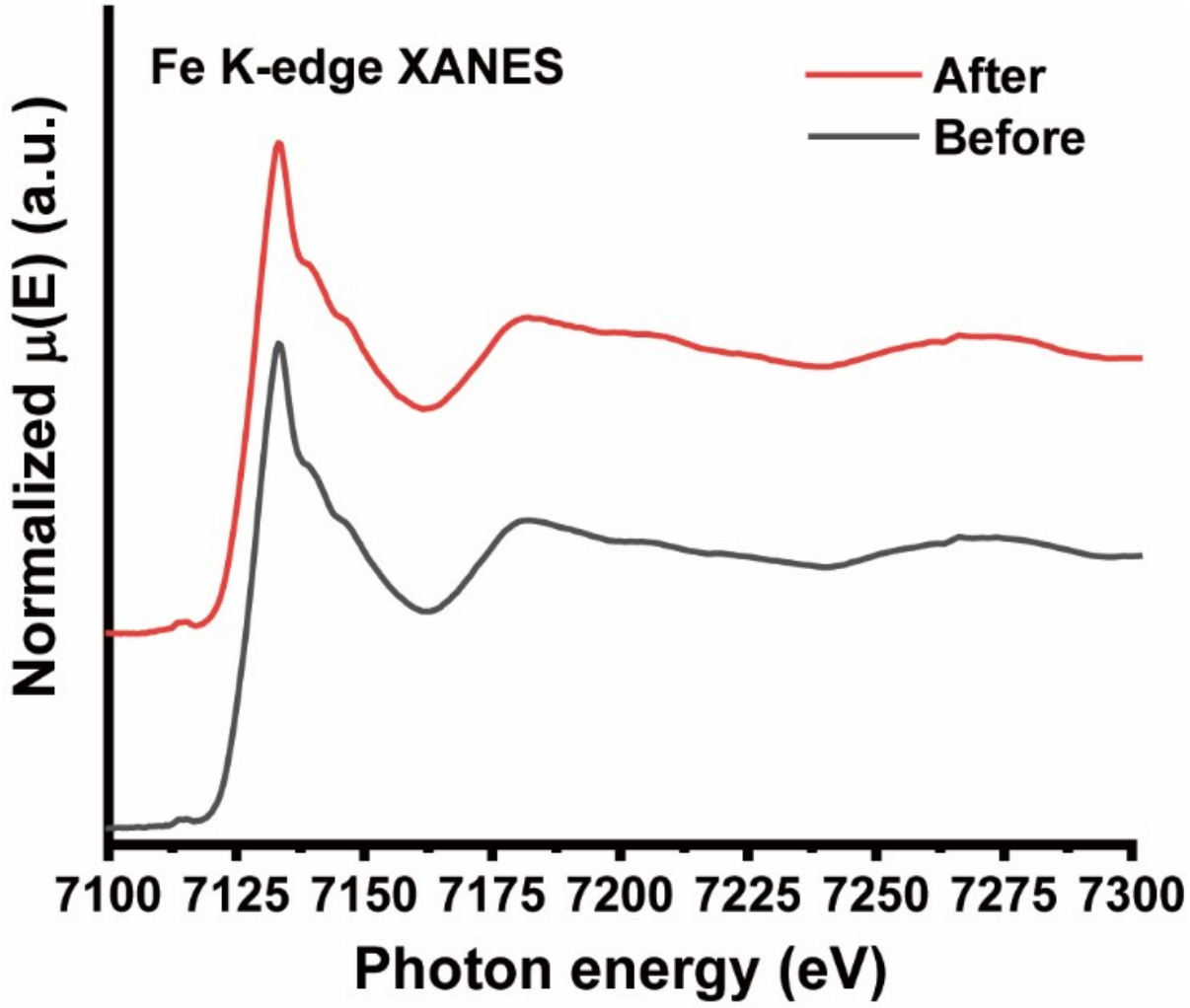

Fig. S15 | Ex-situ Fe K-edge XANES spectrum before/after electrochemical nitrate reduction. The after-RXN sample has analysed after 1 cycle of the electrochemical reaction conducted by chronoamperometric technique for an hour at –0.2 V (vs RHE) in 1 M KOH with 5 mM of KNO_3.

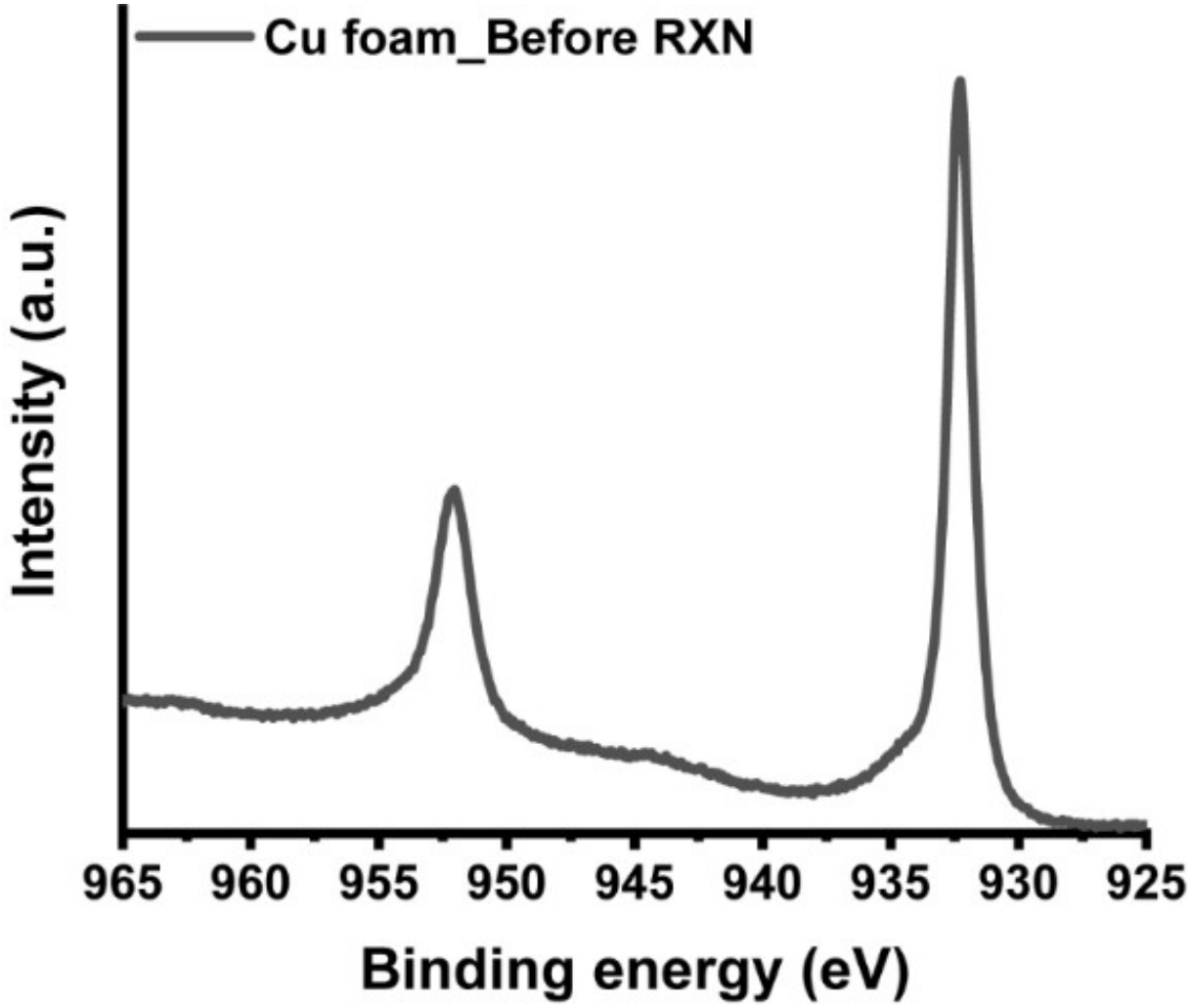

Fig. S16 | Cu 2p XPS for Cu foam electrode.

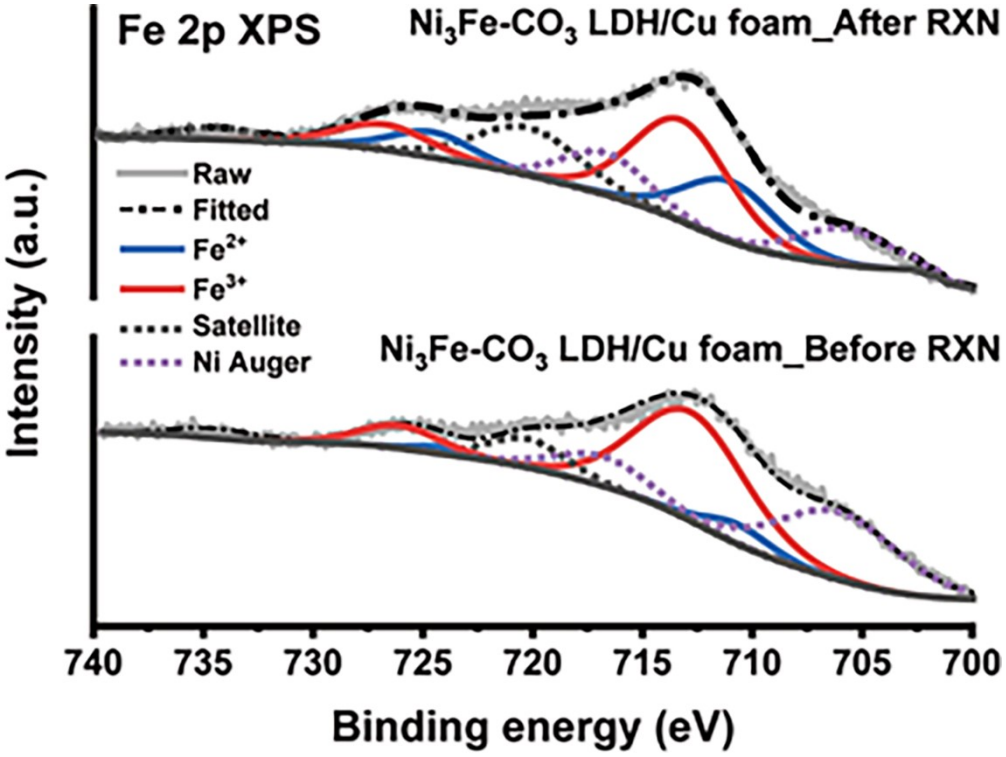

Fig. S17 | Fe 2p XPS for the Ni_3Fe-CO_3 LDH/Cu foam electrode before/after electrochemical nitrate reduction. The after-RXN sample has analysed after 1 cycle of electrochemical reaction conducted by chronoamperometric technique for an hour at –0.2 V (vs RHE) in 1 M KOH with 5 mM of KNO_3.

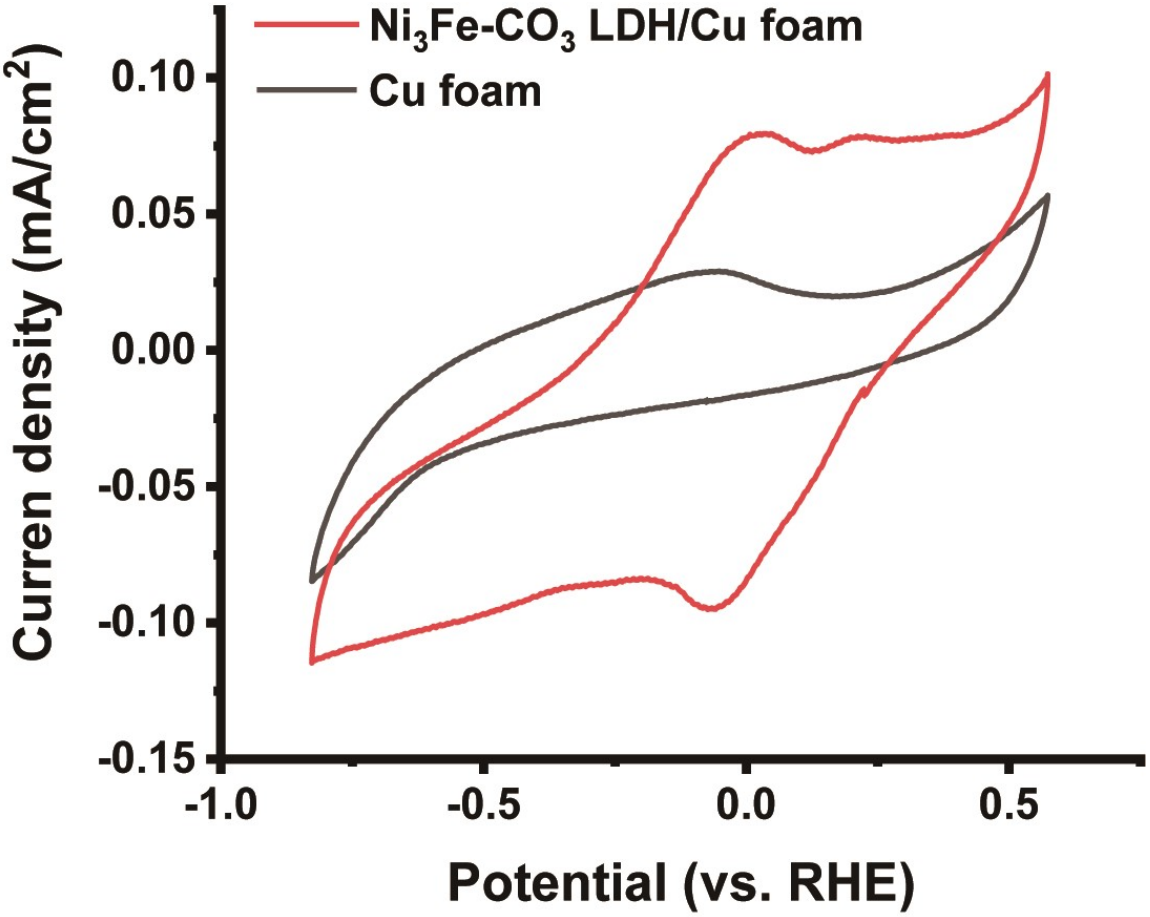

Fig. S18 | CV curves for Ni_3Fe-CO_3 LDH/Cu foam and Cu foam under 1M KOH.

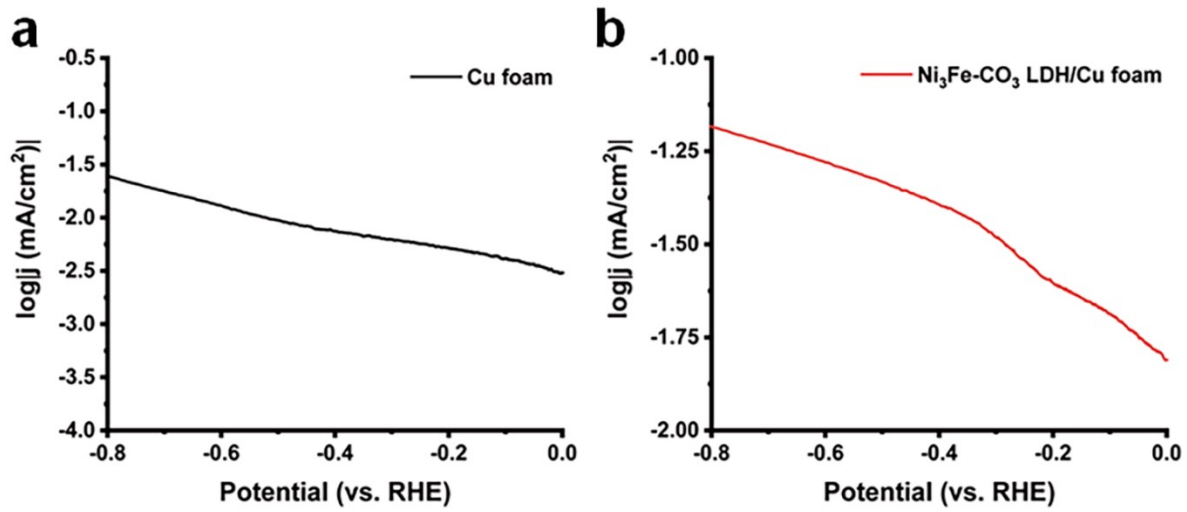

Fig. S19 | Tafel slopes for Ni_3Fe-CO_3 LDH/Cu foam and Cu foam under 1M KOH.

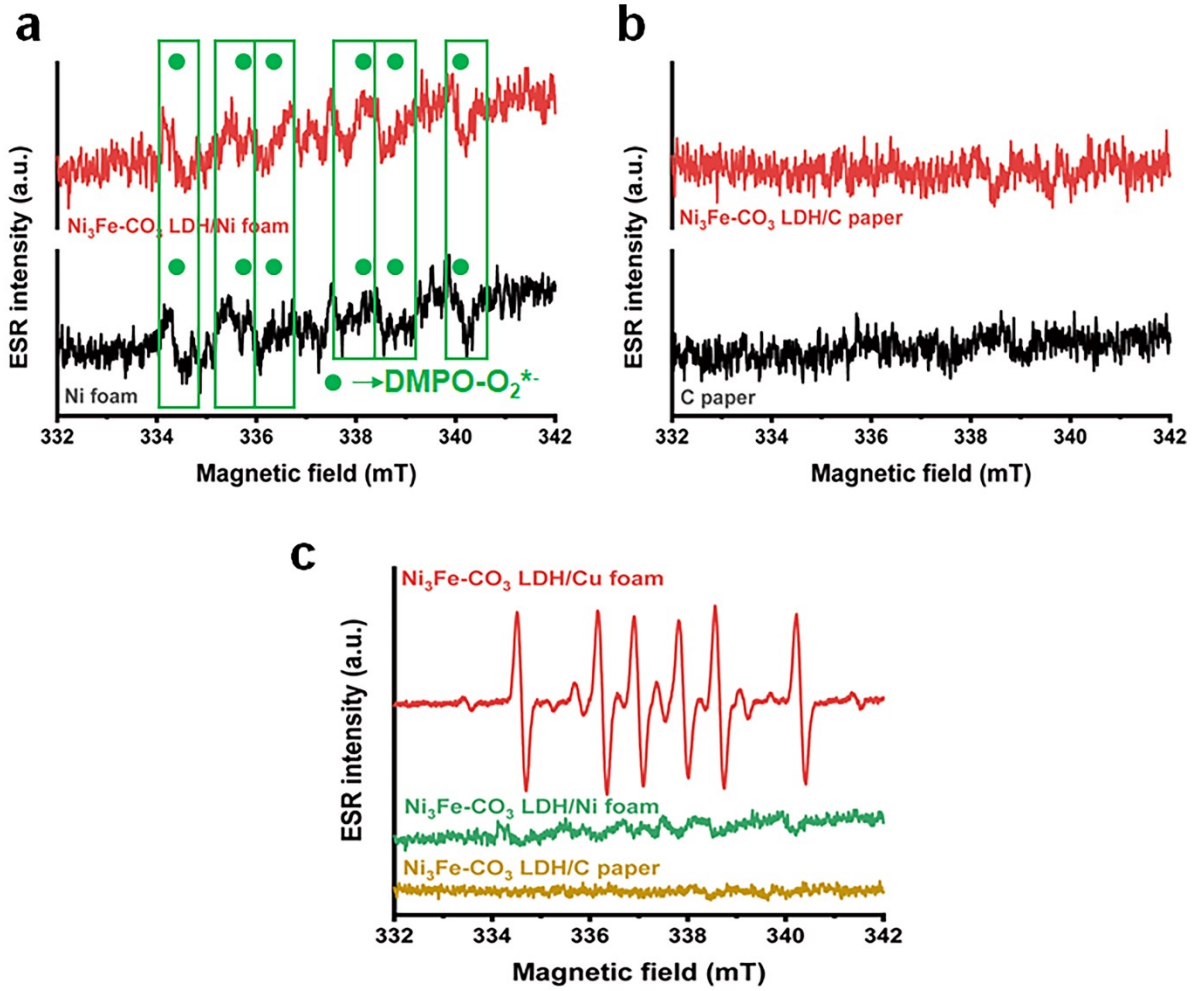

Fig. S20 | ESR spectra of the solutions obtained by (a) the Ni_3Fe-CO_3 LDH/Ni foam, Ni foam electrodes, (b) the Ni_3Fe-CO_3 LDH/C paper and C paper in presence of 50 mM DMPO in 1 M KOH. (c) ESR spectra comparison depending on the different supporting materials. The electrochemical reaction was conducted by chronoamperometric technique for an hour to trap the radicals.

VI. Supplementary table

Table S1 | Lattice parameters and basal spacing for the synthesised LDHs.

Sample	d_{003} (Å)	Lattice parameters (Å)[a]		Crystal domain size (Å)	
		a	*c*	*c*-axis	*ab*-plane
$Ni_3Al\text{-}CO_3$	7.76	3.04	23.28	182.60	223.66
$Ni_3V\text{-}CO_3$	7.56	3.08	22.66	68.78	134.36
$Ni_3Fe\text{-}CO_3$	7.83	3.09	23.48	122.38	184.56
$Ni_3Co\text{-}CO_3$	7.88	3.12	23.65	44.75	134.36
$Co_3Al\text{-}CO_3$	7.70	3.08	23.10	131.23	170.86
$Co_3V\text{-}CO_3$	7.71	3.12	23.12	119.43	231.87
$Co_3Fe\text{-}CO_3$	7.61	3.12	22.82	174.75	276.06
$Zn_3Al\text{-}CO_3$	7.62	3.07	22.85	172.83	275.69
$Zn_3V\text{-}CO_3$	6.89	3.10	20.66	194.07	281.32
$Zn_3Fe\text{-}CO_3$	6.92	3.19	20.77	115.51	288.68
$Mg_3Al\text{-}CO_3$	7.74	3.05	23.21	137.58	207.63
$Mg_3Fe\text{-}CO_3$	7.83	3.11	23.48	177.14	259.91

[a] Indexed to unit cell, $a = b \neq c$; $\alpha = \beta = \gamma = 90°$

Table S2 | Fitted resistance results from Nyquist plots in Fig. 4b.

Resistance	Analysis condition	
	Ni_3Fe-CO_3 LDH/Cu foam (Ω)	Cu foam (Ω)
R_1	0.576	1.123
R_2	0.277	3.658
R_3	1.789	n/a

Table S3 | NO_3^- concentration, operating voltage, faradaic efficiency and half-cell energy efficiency in Fig. 5e.

# of reference	Catalyst/ electrode	NO_3^- conc. (mM)	Operating voltage (V vs RHE)	Faradaic efficiency (%)	Energy efficiency (%)
5	Fe single atom/glassy carbon	500	–0.66	75.0	21.4
10	CoP NAs/carbon fiber cloth	1000	–0.30	97.5	34.4
13	BCN@Cu/carbon paper	100	–0.60	88.9	26.2
14	Pd doped TiO_2/carbon cloth	250	–0.70	92.1	25.8
15	Fe cyano-coordinated polymer NSs/carbon fiber paper	100	–0.50	90.2	30.6
16	$NiCo_2O_4$ NW/carbon cloth	100	–0.60	95.0	28.0
18	CoO_x/carbon cloth	200	–0.30	93.4	33.0
20	Pd onto Vulcan carbon/glassy carbon	20	–0.20	35.1	13.25
23	Co deoped Fe/Fe_2O_3/Ni foam	5	–0.74	85.2	23.3
24	Pd-Cu_2O CEO/carbon paper	0.5	–0.64	96.6	27.8
39	Cu/Cu_2O NWAs/Cu mesh	2	–0.85	95.8	24.9
43	CoFe LDH/Ni foam	14	–0.45	97.7	31.4
44	Cu-PTCDA/carbon cloth	5	–0.40	85.9	28.5
45	TiO_{2-x}/carbon paper	0.5	–0.94	85.0	21.1
46	Fe doped Cu/glassy carbon	2	–0.74	94.5	25.9
47	Cu_2O/Cu/carbon felt	2.5	–0.25	84.4	30.8
48	Ru_xO_y onto Ni-MOF/Ni foam	0.5	–0.30	73.0	25.8
53	CoAl LDH/carbon cloth	100	-0.7	82.1	22.9
This work		5	–0.20	96.8	36.6